Energy & Environmental Science

PAPER

View Article Online
View Journal | View Issue



Cite this: *Energy Environ. Sci.*, 2014, **7**, 1148

# Rate limiting interfacial hole transfer in $Sb_2S_3$ solid-state solar cells†

Jeffrey A. Christians,‡ David T. Leighton, Jr. and Prashant V. Kamat‡§*

Received 25th November 2013
Accepted 27th January 2014

DOI: 10.1039/c3ee43844a

www.rsc.org/ees

Transfer of photogenerated holes from the absorber species to the p-type hole conductor is fundamental to the performance of solid-state sensitized solar cells. In this study, we comprehensively investigate hole diffusion in the $Sb_2S_3$ absorber and hole transfer across the $Sb_2S_3$–CuSCN interface in the $TiO_2$–$Sb_2S_3$–CuSCN system using femtosecond transient absorption spectroscopy, carrier diffusion modeling, and photovoltaic performance studies. Transfer of photogenerated holes from $Sb_2S_3$ to CuSCN is found to be dependent on $Sb_2S_3$ film thickness, a trend attributed to diffusion in the $Sb_2S_3$ absorber. However, modeling reveals that this process is not adequately described by diffusion limitations alone as has been assumed in similar systems. Therefore, both diffusion and transfer across the $Sb_2S_3$–CuSCN interface are taken into account to describe the hole transfer dynamics. Modeling of diffusion and interfacial hole transfer effects reveal that interfacial hole transfer, not diffusion, is the predominant factor dictating the magnitude of the hole transfer rate, especially in thin (<20 nm) $Sb_2S_3$ films. Lastly, the implications of these results are further explored by photovoltaic measurements using planar $TiO_2$–$Sb_2S_3$–CuSCN solar cells to elucidate the role of hole transfer in photovoltaic performance.

**Broader context**

Solid-state sensitized solar cells (SSCs) utilizing semiconductor absorbers overcome the issues of leakage and evaporation encountered in liquid-junction SSCs, and offer the potential for efficient, low cost photovoltaics. For widespread commercialization these solar cells require higher power conversion efficiency than is currently obtained with state-of-the-art devices. One critical component to this is the efficient extraction of photogenerated charges from the semiconductor absorber material. In this study, we decouple the two steps of hole transfer in the $Sb_2S_3$–CuSCN system: diffusion of holes in the $Sb_2S_3$ absorber layer, and transfer of these holes across $Sb_2S_3$–CuSCN interface. We find that interfacial transfer is the major limiting step in the thin (<20 nm) $Sb_2S_3$ films used for high efficiency $Sb_2S_3$ photovoltaics. Decoupling of diffusion and interfacial transfer leads to a deeper understanding of the mechanism of hole transfer in solid-state solar cells. This information has implications for the future design of semiconductor-based SSCs as it points to an important, often neglected interface, the absorber–hole conductor interface, which can play an important role in charge extraction.

## Introduction

In the search for renewable carbon-neutral energy, sensitized solar cells (SSCs) have been widely studied as they offer the potential for inexpensive, highly efficient photovoltaics.[1–4] These solar cells rely on the rapid transfer of photogenerated electrons and holes to an electron acceptor (typically $TiO_2$ or ZnO) and a hole acceptor (liquid redox couple or solid hole conductor) from the sensitizer (dye or semiconductor) to achieve efficient charge separation and extraction.[4–6] Solid-state SSCs are of particular interest because of electrolyte leakage issues that have hindered the commercial prospects of liquid-junction SSCs.[6–8] A wide variety of semiconductor sensitizers have been employed in solid-state SSCs including, CdSe,[9–11] CdS,[12] $In_2S_3$,[13] and $Sb_2S_3$.[14–20] Of these sensitizer materials, $Sb_2S_3$ shows particular promise, providing reported efficiencies of 3.1%,[18] 4.1%,[19] 5.13%,[20] and 6.3%[14] using spiro-OMeTAD, CuSCN, P3HT, and PCPDTBT–PCBM hole conductors, respectively. In addition, crystalline $Sb_2S_3$ has a band gap of 1.7–1.8 eV,[21] allowing for absorption across the visible spectrum, and indicating that even higher efficiencies than those reported are achievable using $Sb_2S_3$.[8]

Because the charge separation process in SSCs is dictated by the relative rates of charge transfer and recombination, knowledge of these rates is of great importance for the design of higher efficiency devices.[22,23] Toward this goal, we recently reported on the mechanism and rate of hole transfer between $Sb_2S_3$ and CuSCN.[24] This previous work elucidated the two-step

*Department of Chemical and Biomolecular Engineering, University of Notre Dame, Notre Dame, Indiana 46556, USA. E-mail: pkamat@nd.edu*

† Electronic supplementary information (ESI) available: Included are control femtosecond transient absorption experiments using $TiO_2$, CuSCN, and $TiO_2$–CuSCN films, and a complete derivation of hole transfer kinetic model along with necessary assumptions. See DOI: 10.1039/c3ee43844a

‡ Radiation Laboratory, University of Notre Dame, Notre Dame, Indiana 46556, USA.

§ Department of Chemistry and Biochemistry, University of Notre Dame, Notre Dame, Indiana 46556, USA.

nature of the hole transfer process by following the spectroscopic fingerprint of trapped holes ($S^{-\bullet}$ radical) in the $Sb_2S_3$. The present study expands on this previous work by investigating the diffusion of holes in the $Sb_2S_3$, and how this influences the hole transfer rate from $Sb_2S_3$ to CuSCN.

Minority carrier diffusion length, $L_D$, is an important parameter that aids in the determination of optimal solar cell architecture as it dictates the critical absorber dimension beyond which charges are no longer extracted efficiently.[25–33] For example, low diffusion lengths seen in organic photovoltaics (typically $L_D$ < 20 nm) necessitate the interpenetrating donor/acceptor network employed in bulk heterojunctions to optimize both charge extraction and light absorption.[25,29,34] On the other hand, semiconductors, such as lead sulfide[31] and lead halide perovskite,[26,27] exhibit $L_D$ from tens of nanometers to over a micron. This allows for the design of mesostructured extremely thin absorber,[5,16,35] and planar heterojunction[36,15] solar cells with efficient charge extraction.

For these reasons, the diffusion of $S^{-\bullet}$ in $Sb_2S_3$ is investigated by observing the decrease in the observed hole transfer rate to CuSCN as a function of increasing $Sb_2S_3$ thickness. Traditionally, diffusion in this type of system is modeled using an absorbing boundary condition which assumes infinitely fast transfer across the donor/acceptor interface (*i.e.* hole concentration goes to zero at this interface).[26,27,33,34] However, herein we provide evidence that interfacial hole transfer also limits the hole transfer rate from $Sb_2S_3$ to CuSCN. Therefore, a model is developed describing the balance between hole diffusion in the $Sb_2S_3$ layer and transfer across the $Sb_2S_3$–CuSCN interface, and the results are compared to the standard diffusion model employing absorbing boundary conditions. The diffusion-transfer model developed provides a better picture of the hole dynamics in $Sb_2S_3$ than the traditional diffusion model. Also, taking interfacial transfer resistance into account provides a better estimate of the intrinsic properties of the $Sb_2S_3$ absorber. Conversely, the diffusion only model is able to accurately estimate such device parameters as the productive absorber thickness. Together, these two models provide complementary information that serves to elucidate the limitations and mechanism of hole transfer in $Sb_2S_3$ solar cells. Finally, these results are correlated to planar $TiO_2$–$Sb_2S_3$–CuSCN photovoltaics, highlighting the importance of hole transfer to overall photovoltaic performance. These results offer a comprehensive understanding of the balance between hole diffusion and interfacial transfer and its effect on $Sb_2S_3$ photovoltaic performance.

## Results and discussion

### Experimental measurements of $Sb_2S_3$–CuSCN hole transfer

To investigate the correlation between $Sb_2S_3$ film thickness and hole transfer, $TiO_2$–$Sb_2S_3$ and $TiO_2$–$Sb_2S_3$–CuSCN films were prepared with varying $Sb_2S_3$ layer thickness. $Sb_2S_3$ films (20–130 nm) were deposited by chemical bath deposition on planar $TiO_2$ substrates. In contrast to the mesoporous $TiO_2$ substrates used in high efficiency $Sb_2S_3$ solar cells, planar $TiO_2$ substrates were employed to allow for precise control of $Sb_2S_3$ thickness (Fig. 1A). The amorphous, as-deposited $Sb_2S_3$ was annealed under nitrogen to obtain crystalline $Sb_2S_3$. As shown in Fig. 1B, the thickness of the $Sb_2S_3$ layer was calculated from the absorption coefficient of the $Sb_2S_3$ films at 450 nm ($\alpha = 1.5 \times 10^5$).[24] Following characterization of $TiO_2$–$Sb_2S_3$ films, CuSCN was applied after KSCN treatment using a homemade automated deposition apparatus as described in the Experimental Methods.

Transient absorption spectroscopy is a useful tool to probe the recombination dynamics of semiconductor systems, and can be used to extract information about electron transfer reactions occurring in the system. Time-resolved difference absorption spectra of the $Sb_2S_3$ films described above were recorded over the time window of 0–1500 ps following a 387 nm laser pulse excitation. Transient absorption spectra of all films studied show three distinct features: an induced absorption peak at 560 nm attributed to the absorption of $S^{-\bullet}$ arising from trapped holes in the $Sb_2S_3$, and two photobleaching maxima at 460 nm and 650 nm attributed to the photobleaching of the first and second excitonic peaks in the steady-state absorption spectra. Absorption difference spectra of $TiO_2$–$Sb_2S_3$ and $TiO_2$–$Sb_2S_3$–CuSCN films with a 34 nm $Sb_2S_3$ layer are shown in Fig. 2A and B, respectively. As detailed in our previous work,[24] hole transfer from $Sb_2S_3$ to CuSCN occurs *via* a two-step trap and transfer mechanism. Initially, photogenerated holes are trapped in $Sb_2S_3$ (reaction (1)). These trapped holes are localized on one of the $Sb_2S_3$ sulfur atoms which gives rise to a spectral signal indicative of a S-radial anion ($S^{-\bullet}$). This trapped hole is subsequently shown as $S^{-\bullet}$ (or $Sb_2S_2S^{-\bullet}$ when referring to it in the $Sb_2S_3$ crystal lattice). These trapped holes are then transferred from $Sb_2S_3$ to CuSCN (reaction (2)) which results in the decay of the $S^{-\bullet}$ induced absorption.

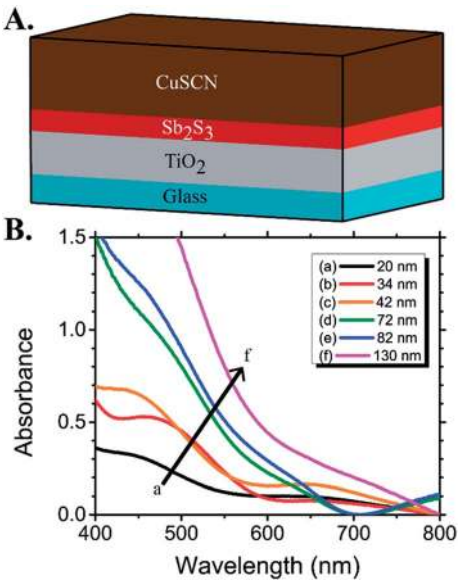


Fig. 1 (A) Scheme showing planar $TiO_2$–$Sb_2S_3$–CuSCN film used for transient absorption spectroscopy. (B) UV-visible absorption spectra of $TiO_2$–$Sb_2S_3$ films used in transient absorption spectroscopy with corresponding thickness of the $Sb_2S_3$ layer calculated from the film absorption at 450 nm.

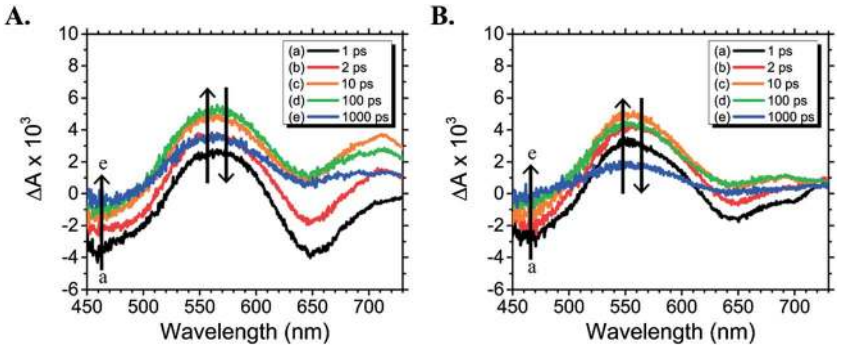


Fig. 2 Time-resolved difference absorption spectra obtained (a) 1 ps, (b) 2 ps, (c) 10 ps, (d) 100 ps, and (e) 1000 ps following a 387 nm laser pulse excitation of (A) $TiO_2$–$Sb_2S_3$ and (B) $TiO_2$–$Sb_2S_3$–CuSCN films in vacuum. Thickness of the $Sb_2S_3$ layer was measured as 34 nm.

$$Sb_2S_3\ (h) \xrightarrow{k_{trap}} Sb_2S_2S^{-\cdot} \quad (1)$$

$$Sb_2S_2S^{-\cdot} + CuSCN \xrightarrow{k_{ht}} Sb_2S_3 + Cu(SCN^{-\cdot}) \quad (2)$$

Based on previous studies of metal–chalcogenide semiconductor systems, the trapping of photogenerated charges is expected to take place on the surface of the $Sb_2S_3$ crystals.[37] The rate of hole trapping in $Sb_2S_3$ is independent of film thickness, as seen by the growth of the $S^{-\cdot}$ absorption at 560 nm in Fig. 3A. Hole trapping is also seen to be independent of the presence of CuSCN as shown in Fig. 3B. This indicates that $S^{-\cdot}$ formation does not occur primarily at the $Sb_2S_3$ surface or at the $Sb_2S_3$–CuSCN interface. Instead, this trapping may occur in the bulk crystallite through the breaking of the weak Sb–S bonds in the $Sb_2S_3$ lattice.[38,24] Thus, it can be assumed that photogenerated holes are trapped as $S^{-\cdot}$ at or near the point of generation in the $Sb_2S_3$ film, which implies that they must diffuse to the $Sb_2S_3$–CuSCN interface before transfer to CuSCN.

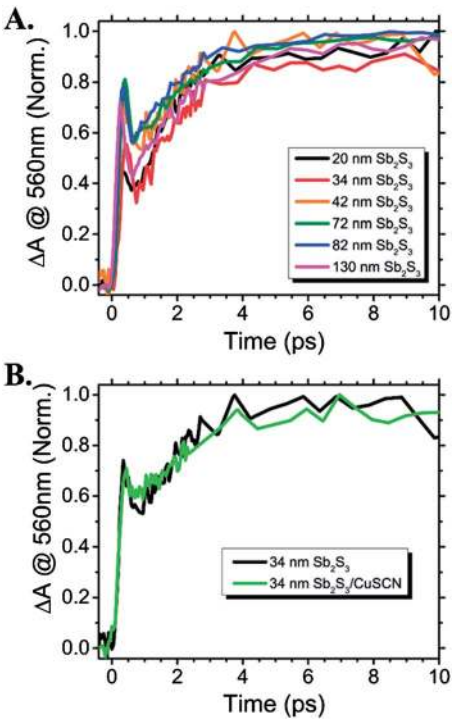


Fig. 3 (A) Transient kinetic trace showing the rise time of the 560 nm $S^{-\cdot}$ induced absorption in the absence of hole scavenger for $Sb_2S_3$ films of varying thickness and (B) a 34 nm $Sb_2S_3$ film with and without CuSCN.

Hole transfer rates were calculated by comparing the decay of the $S^{-\cdot}$ absorption in the presence and absence of CuSCN. Recently, O'Mahony *et al.* showed that an electron acceptor in not required for efficient hole extraction, and that charge separation may be initiated by hole extraction.[22] Therefore, in the case of $TiO_2$–$Sb_2S_3$ films without CuSCN, we attribute the decay of trapped holes (*viz.* the $S^{-\cdot}$ species) to non-radiative electron–hole recombination (reaction (3)). The addition of CuSCN opens an additional decay pathway, transfer of holes to CuSCN (reaction (2)), which is expected to increase the rate of the $S^{-\cdot}$ decay.

$$Sb_2S_2S^{-\cdot} + e^- \rightarrow Sb_2S_3 + \text{heat} \quad (3)$$

Kinetic traces of the decay of the $S^{-\cdot}$ at 560 nm were assembled from the time-resolved transient absorption spectral data and modeled using a triexponential model (eqn (4)).

$$y = C\,[-e^{(-t/\tau_1)} + A\,e^{(-t/\tau_2)} + (1 - A)e^{(-t/\tau_3)}] \quad (4)$$

These fits yielded an exponential saturation ($\tau_1$), a short ($\tau_2$) and long ($\tau_3$) decay lifetime, a weighted coefficient ($A$) representing the contribution of the decay lifetimes to the overall transient signal decay, and the magnitude of the induced absorption signal ($C$). It is assumed that the transient kinetics of the varying thicknesses of $Sb_2S_3$ films are identical as all films studied are thick compared to the exciton Bohr radius of $Sb_2S_3$.[39] Therefore, the kinetic lifetimes ($\tau_1$, $\tau_2$, and $\tau_3$) and weighting coefficient ($A$) used were determined from all $TiO_2$–$Sb_2S_3$ films simultaneously, while the signal magnitude ($C$) was allowed to vary between kinetic traces. This fitting was found to adequately describe the kinetics of the induced absorption signal for all $TiO_2$–$Sb_2S_3$ films studied. The largest discrepancy was seen for the 20 nm thick $Sb_2S_3$ film; however, the low transient absorption signal and potential residual absorptions complicates the fitting of this film. The exponential growth ($\tau_1 = 1.26$ ps) of the $S^{-\cdot}$ induced absorption is attributed to hole

 

trapping (reaction (1)). Subsequently, holes undergo two decay pathways: a fast process ($\tau_2 = 184$ ps) responsible for 20% of the decay, and a slow pathway ($\tau_3 = 4.7$ ns) responsible for 80% of the observed decay. The presence of a biexponential hole decay indicates that there are two distinct trapped hole species in the $Sb_2S_3$, one short-lived and another long-lived species. Future work is needed to better understand and suppress the mechanism by which the short-lived holes recombine to further improve charge collection.

Because hole trapping occurs at least two orders of magnitude faster than either recombination or transfer, and is not affected by CuSCN, kinetic modeling of $TiO_2$–$Sb_2S_3$–CuSCN was done following the completion of hole trapping ($t > 6$ ps) for simplicity. Therefore, $TiO_2$–$Sb_2S_3$–CuSCN kinetic traces were fit to a biexponential equation (eqn (5)).

$$y = C\,[A\,e^{(-t/\tau_2)} + (1 - A)e^{(-t/\tau_3)}] \quad (5)$$

where $C$ is the magnitude of the response, $A$ is the weight and $\tau_2$ is the lifetime of the short component of the decay, and $\tau_3$ is the long component lifetime. Because the $Sb_2S_3$ films are different thicknesses, it is anticipated that the decay kinetics will vary between films due to differences in hole transfer, so all parameters were allowed to vary in order to best fit each transient kinetic trace.

The fitting parameters of all films studied are summarized in Table 1, and the transient kinetic data with fits are shown in Fig. 4A–C. For $TiO_2$–$Sb_2S_3$ films, the short and long lifetimes of the $S^{-\bullet}$ absorption decay are attributed to non-radiative electron–hole recombination (reaction (3)), while for $TiO_2$–$Sb_2S_3$–CuSCN films it is attributed to both electron–hole recombination and hole transfer to CuSCN (reaction (2) and (3)). To decouple recombination and hole transfer, it is assumed that there is no difference in the recombination dynamics in films with and without CuSCN. From this assumption, the estimated rate of hole transfer, $k_{ht}$, from $Sb_2S_3$ to CuSCN can be calculated from the average lifetime of the $S^{-\bullet}$ absorption by eqn (6):

$$k_{ht} = 1/\langle\tau\rangle_{Sb_2S_3/CuSCN} - 1/\langle\tau\rangle_{Sb_2S_3} \quad (6)$$

where $k_{ht}$ is the estimated hole transfer rate, and $\langle\tau\rangle_{Sb_2S_3/CuSCN}$ and $\langle\tau\rangle_{Sb_2S_3}$ are the average lifetimes of the decay in the presence and absence of CuSCN, respectively. Unlike the case without CuSCN where a single set of parameters described the dynamics of all $Sb_2S_3$ film thicknesses, we find that the presence of CuSCN requires $A$, $\tau_2$, and $\tau_3$ to vary. As a result the estimated hole transfer rate, $k_{ht}$, is found, as shown in Fig. 5, to be dependent on $Sb_2S_3$ film thickness. It is expected that the primary reason hole transfer rate decreases with increasing film thickness is the diffusion of photogenerated holes from their point of generation in the $Sb_2S_3$ film to the $Sb_2S_3$–CuSCN interface.

Taken as a whole, the proposed mechanism for hole transfer is as follows: (i) laser pulse excitation creates photogenerated holes in $Sb_2S_3$. (ii) Photogenerated holes are trapped in two distinct trap sites with approximately 20% of holes trapped in short-lived states and 80% in long-lived states. (iii) Short and long-lived holes recombine with exponential time constants estimated as 184 ± 45 ps and 4.7 ± 0.7 ns, respectively. (iv) In addition to recombination, holes diffuse *via* a random walk through the $Sb_2S_3$ film to the $Sb_2S_3$–CuSCN interface (reaction (7)) where, (v) they then can be transferred across this interface into CuSCN (reaction (8)).

$$Sb_2S_2S^{-\bullet} + CuSCN \rightarrow [Sb_2S_2S^{-\bullet} - CuSCN] \quad (7)$$

$$[Sb_2S_2S^{-\bullet} - CuSCN] \rightarrow Sb_2S_3 + Cu(SCN^{-\bullet}) \quad (8)$$

While it is traditionally assumed that the rate of interfacial transfer (reaction (8)) is much faster than hole diffusion (reaction (7)), this is not necessarily the case. Therefore, the contribution by each of these processes was studied in detail. To do this we employ two distinct hole transfer models: one which includes both diffusion and interfacial hole transfer, and a second that considers only hole diffusion in the $Sb_2S_3$ sensitizer. In the following sections the results of these two models are compared in detail.

### Modeling diffusion and interfacial transfer

Initially, we consider the case where both hole diffusion in $Sb_2S_3$ and hole transfer across the $Sb_2S_3$–CuSCN interface contribute to the observed hole transfer dynamics. Hole diffusion and interfacial transfer were modeled by the idealized system shown in Fig. 6.[33,41,42] It was assumed that the diffusion of holes is described by a one-dimensional random walk and they are removed from the $Sb_2S_3$ layer by either transfer to CuSCN, or electron–hole recombination. Recombination is assumed to act homogeneously throughout the $Sb_2S_3$ film and

Table 1 Summary of the results of fitting of induced absorption decay at 560 nm

| Sample[a] | $\tau_1$ (ps) | $A$ | $\tau_2$ (ps) | $\tau_3$ (ps) | $\langle\tau\rangle^b$ (ps) | $k_{ht}$ ($\times 10^8$ s$^{-1}$) |
|---|---|---|---|---|---|---|
| $TiO_2$–$Sb_2S_3$ (20–130 nm) | 1.26 ± 0.02 | 20 ± 2.7% | 184 ± 45 | 4680 ± 700 | 4630 ± 700 | — |
| $TiO_2$–$Sb_2S_3$ (20 nm)–CuSCN | — | 66 ± 27% | 210 ± 80 | 960 ± 670 | 730 ± 370 | 11.5 ± 6.0 |
| $TiO_2$–$Sb_2S_3$ (34 nm)–CuSCN | — | 18 ± 2.8% | 90 ± 24 | 1110 ± 56 | 1090 ± 50 | 7.0 ± 1.1 |
| $TiO_2$–$Sb_2S_3$ (42 nm)–CuSCN | — | 19 ± 4.8% | 130 ± 51 | 1300 ± 120 | 1280 ± 103 | 5.7 ± 1.0 |
| $TiO_2$–$Sb_2S_3$ (72 nm)–CuSCN | — | 31 ± 4.5% | 160 ± 38 | 2170 ± 310 | 2100 ± 290 | 2.6 ± 0.5 |
| $TiO_2$–$Sb_2S_3$ (82 nm)–CuSCN | — | 29 ± 7.4% | 240 ± 77 | 2480 ± 550 | 2390 ± 500 | 2.0 ± 0.5 |
| $TiO_2$–$Sb_2S_3$ (130 nm)–CuSCN | — | 25 ± 11% | 170 ± 110 | 2160 ± 660 | 2100 ± 600 | 2.6 ± 0.8 |

[a] Thickness of the $Sb_2S_3$ film as estimated by UV-visible absorption is shown in parenthesis. [b] Average lifetime $\langle\tau\rangle$ is calculated by the equation:[40] $\langle\tau\rangle = (A\tau_2^2 + (1 - A)\tau_3^2)/(A\tau_2 + (1 - A)\tau_3)$.

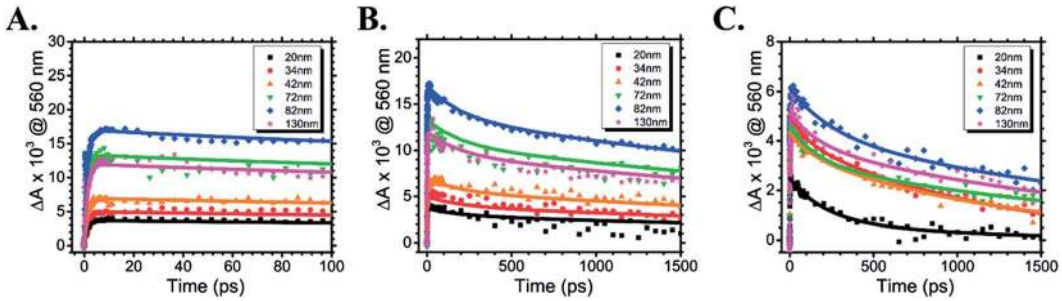


Fig. 4 Transient kinetic traces showing the decay of the $S^{-\bullet}$ induced absorption peak at 560 nm fit using a triexponential equation (eqn (4)). Fits for $TiO_2$–$Sb_2S_3$ films shown on short (A) and long (B) timescales. Fits for $TiO_2$–$Sb_2S_3$–CuSCN films shown at long (C) timescales.

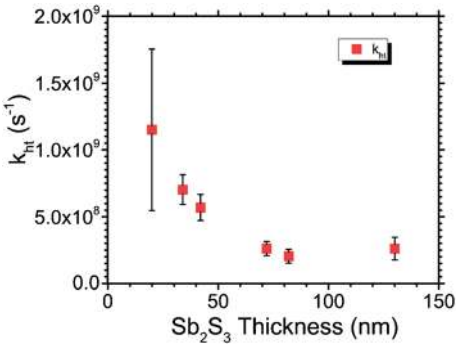


Fig. 5 Trace showing how the estimated hole transfer rate calculated decreases with increasing $Sb_2S_3$ film thickness. Error bars represent the error in $k_{ht}$ as calculated from the error of the fitting parameters as shown in Table 1.

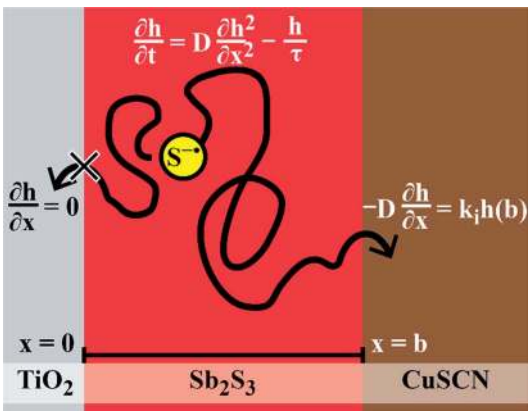


Fig. 6 (A) Scheme showing the $TiO_2$–$Sb_2S_3$–CuSCN system modeled using Fick's second law of diffusion with appropriate boundary conditions.

independently from diffusion and transfer. As previously discussed, there are two distinct hole species in the $Sb_2S_3$, one short-lived ($h_s$) and another long-lived ($h_l$). The short-lived holes make up a small proportion of the total trapped holes (20%), and decay rapidly by recombination. This means that these do not contribute significantly to the overall transfer process, so the results of the subsequent model are primarily influenced by long-lived holes. Therefore, the problem is simplified by assuming that there is no difference between $h_s$ and $h_l$ other than recombination rate. As previously, kinetic modeling was simplified by only looking at the decay following completion of hole trapping ($t > 6$ ps).

From these assumptions, the concentration of holes in $Sb_2S_3$ in the $Sb_2S_3$–CuSCN films can be described as the linear combination of the contributions of short-lived and long-lived holes, ($h = h_s + h_l$) where each species can be described by a modified Fick's second law of diffusion as shown for $h_l$ in eqn (9).

$$\frac{\partial h_l}{\partial t} = D\frac{\partial^2 h_l}{\partial x^2} - \frac{h_l}{\tau_3} \tag{9}$$

where $h_l$ is the concentration of the long-lived holes in $Sb_2S_3$ in the $TiO_2$–$Sb_2S_3$–CuSCN films, $D$ is the effective hole diffusion coefficient, and $\tau_3$ is the lifetime derived from the fitting of the kinetics of $TiO_2$–$Sb_2S_3$ films in the absence of CuSCN, shown in Table 1. Since it is assumed that short-lived and long-lived holes only differ in their respective lifetime, we will only develop the solution for $h_l$ in detail. As an initial condition, we assume trapped holes are distributed exponentially throughout the $Sb_2S_3$ film (eqn (10)), where $\alpha$ is the absorption coefficient at the 387 nm excitation wavelength. For boundary conditions, we assume that there is no hole transfer between the $Sb_2S_3$ and $TiO_2$ (eqn (11)), and that the flux of holes across the $Sb_2S_3$–CuSCN heterojunction is pseudo first order with respect to the concentration of holes at the interface (eqn (12)), where $k_i$ is the proportionality constant or interfacial hole transfer coefficient.

$$h_l|_{t=0} = (1 - A)h_0 e^{-\alpha x};\ 0 \le x \le b \tag{10}$$

$$\left.\frac{\partial h_l}{\partial x}\right|_{x=0} = 0; \quad t > 0 \tag{11}$$

$$-D\left.\frac{\partial h_l}{\partial x}\right|_{x=b} = k_i h_l\Big|_{x=b}; \quad t > 0 \tag{12}$$

Solving this problem for the concentration of long-lived holes yields the infinite sum shown in eqn (13), where $\sigma_n$ is $n^{th}$ eigenvalue of the eigenfunction shown in eqn (14), and the constants $B_n$ are derived from the initial condition. The solution for short-lived holes, $h_s$, is analogous to this solution as described in detail in the ESI.†

 

$$h_l = (1-A)e^{-t/\tau_3}\sum_{n=1}^{\infty} B_n e^{-\frac{\sigma_n^2 D}{b^2}t}\cos(\sigma_n x/b) \quad (13)$$

$$\frac{k_i b}{D} = \sigma_n \tan(\sigma_n) \quad (14)$$

Next, in order to fit the experimental transient absorption data, the predicted transient absorption response, $s$, was obtained by integrating the sum of the concentration of short-lived and long-lived holes over the film thickness (eqn (15)). This calculated transient absorption signal (eqn (16)) is used to model the experimental transient kinetic traces to determine the values of $k_i$ and $D$, and takes into account the contributions of both trapped hole species.

$$s = \int_0^b (h_s + h_l)dx \quad (15)$$

$$s = \left[Ae^{-t/\tau_2} + (1-A)e^{-t/\tau_3}\right]\sum_{n=1}^{\infty} B_n \frac{\sin(\sigma_n)}{\sigma_n} e^{-\frac{\sigma_n^2 D}{b^2}t} \quad (16)$$

The parameters $A$, $\tau_2$, and $\tau_3$ are no longer adjustable fitting constants, but rather taken as the fixed values derived from fitting of the $TiO_2$–$Sb_2S_3$ films in the absence of CuSCN. The predicted hole transfer rate, $k_{model}$, is calculated from the hole transfer lifetime of the modeled transient absorption decay, $b^2/\sigma_n{}^2 D$, and the leading coefficients by eqn (17).

$$k_{model} = \left[\sum B_n \frac{\sin(\sigma_n)}{\sigma_n}\left(\frac{b^2}{\sigma_n{}^2 D}\right)^2 \Big/ \sum B_n \frac{\sin(\sigma_n)}{\sigma_n}\left(\frac{b^2}{\sigma_n{}^2 D}\right)\right]^{-1} \quad (17)$$

A full derivation of these solutions, including assumptions, is supplied in the ESI.† Eqn (16) was approximated by the first five terms of the infinite sum ($n = 1$–5), and the model was fit to the transient kinetic decay of $TiO_2$–$Sb_2S_3$–CuSCN films (Fig. 7A) to yield estimates for $D$ and $k_i$. From these values, $k_{model}$ was calculated by eqn (17) as shown in Fig. 7B. An estimate of the random error in the calculated parameters was achieved *via* undersampling of the dataset. From this model, the diffusion coefficient of trapped holes in $Sb_2S_3$ was estimated as $D = 6.8 \pm 4.7 \times 10^{-2}$ cm$^2$ s$^{-1}$, and the interfacial hole transfer coefficient was estimated as $k_i = 2.8 \pm 0.2 \times 10^3$ cm s$^{-1}$. From the calculated diffusion coefficient the mobility of the trapped holes in $Sb_2S_3$ was calculated to be 2.6 ± 1.9 cm$^2$ V$^{-1}$ s$^{-1}$ using the Einstein relation shown in eqn (18).

$$D = \frac{k_B T \mu}{q} \quad (18)$$

where $k_B$ is the Boltzmann constant, $T$ is the temperature, $\mu$ is the carrier mobility, and $q$ is the elementary charge. This hole mobility is ~25% of the reported electron mobility in $Sb_2S_3$ films determined using Hall effect measurements.[43] The high mobility in $Sb_2S_3$ of both electrons and holes is likely a major contributing factor to the high efficiency of $Sb_2S_3$ photovoltaics.

Another important parameter for thin film photovoltaic applications is the minority carrier diffusion length, $L_D$, given by eqn (19).[34]

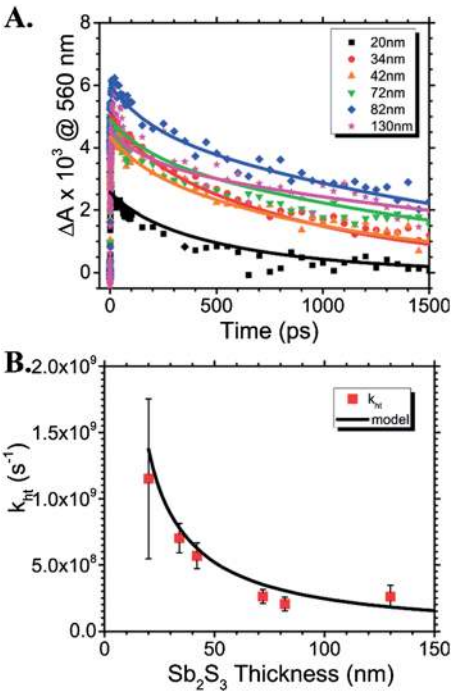


Fig. 7 (A) Plots of transient absorption decay model fit to experimental time resolved transient kinetic data at 560 nm. (B) Plot of modeled & experimentally calculated hole transfer rate *vs.* $Sb_2S_3$ film thickness.

$$L_D = \sqrt{D\tau} \quad (19)$$

where $D$ is the diffusion coefficient, and $\tau$ is the hole lifetime. The average lifetime of the $S^{-\bullet}$ species was determined to be 4.6 ns, as shown in Table 1. From this lifetime, $L_D$ was calculated to be 180 ± 60 nm. Because diffusion and interfacial hole transfer are decoupled in this analysis, $L_D$ provides information on carrier diffusion in $Sb_2S_3$, but overestimates the productive thickness of $Sb_2S_3$ in a photovoltaic device. This overestimation is because interfacial transfer limitations decrease the $Sb_2S_3$ thickness for efficient charge extraction below the diffusion length.

An important parameter obtained from this model is the dimensionless parameter $\lambda$, shown in eqn (20).

$$\lambda = \frac{k_i b}{D} \quad (20)$$

This parameter, referred to as the hole transfer Biot number, is analogous to the Biot number in mass and heat transfer.[44,45] The hole transfer Biot number is the ratio of transfer at the $Sb_2S_3$–CuSCN interface to diffusion in the $Sb_2S_3$. Therefore, the value of $\lambda$ can provide valuable information as to the limiting mechanism in overall hole transfer. If $\lambda \gg 1$, hole diffusion in the $Sb_2S_3$ film (reaction (7)) is much slower than interfacial transfer (reaction (8)), meaning that the overall hole transfer kinetics are primarily limited by diffusion. On the other hand, for $\lambda \ll 1$, diffusion is much faster than interfacial transfer, and hole transfer kinetics are limited by transfer across the $Sb_2S_3$–CuSCN interface. Using the values for $k_i$ and $D$ obtained from the model, $\lambda$ is calculated as $\lambda = 0.10 \pm 0.01$ for 20 nm $Sb_2S_3$

films and $\lambda = 0.64 \pm 0.05$ for 130 nm $Sb_2S_3$ films. As $\lambda < 1$, we find that interfacial transfer plays the major role in dictating the magnitude of the hole transfer rate, although diffusion effects become increasingly important as $Sb_2S_3$ film thickness increases. However, diffusion only becomes the predominant factor in determining hole transport kinetics as film thickness increases beyond 240 nm ($\lambda \approx 1$).

### Modeling diffusion alone

The previous analysis suggests that interfacial transfer is an important factor to consider in the $Sb_2S_3$–CuSCN system. However, in most models of this type, interfacial hole transfer is assumed to be very fast compared to diffusion.[26,27,33,34,41] Therefore, it is of importance to confirm that the previous model is accurate by employing the simplified diffusion-only model. Instead of describing interfacial charge transfer as a pseudo first order process (eqn (12)), the assumption of infinitely fast interfacial transfer defines the concentration of holes at the interface to be zero at all time, $t$ (eqn (21)), analogous to letting $k_i \rightarrow \infty$.

$$h|_{x=b} = 0;\ t > 0 \tag{21}$$

By neglecting the interfacial charge transfer and assigning all contributions to the overall hole transfer kinetics to diffusion, this model provide a lower bound estimate of the diffusion coefficient[27,34,46] that is only accurate in systems where diffusion is very slow compared to interfacial charge transfer (*i.e.* $\lambda \gg 1$). This assumption breaks down when the overall transfer kinetics are significantly influenced by interfacial transfer. This more common model makes a very different assumption of the dynamics of hole transfer than the previously discussed interfacial transfer model. Because of this discrepancy (*viz.* slow interfacial transfer *vs.* infinitely fast interfacial transfer), the results of these two models were compared in detail. This is critical in determining if the data can be adequately explained by this simpler model, or if interfacial hole transfer really does play a major role as asserted.

This new diffusion model was solved analytically as before (eqn (9)) using the absorbing boundary condition (eqn (21)) in place of pseudo first order interfacial transfer (eqn (12)). The solution to this problem is obtained by taking the limit as $k_i \rightarrow \infty$ of eqn (16). This new model was then used to fit the time-resolved absorbance data for the $Sb_2S_3$–CuSCN films to obtain an apparent diffusion coefficient, $D_A$. The apparent diffusion coefficient of holes in $Sb_2S_3$ is estimated as $D_A = 4.3 \pm 0.3 \times 10^{-3}$ $cm^2$ $s^{-1}$ when modeling all films simultaneously. This is an order of magnitude lower than the effective diffusion coefficient calculated when taking interfacial transfer into account using the constant flux boundary condition (eqn (12)). The quality of the fits from the two models were then compared at the two extreme film thicknesses, 20 nm and 130 nm, where interfacial processes have the most and least contribution, respectively (Fig. 8A). It is seen that when a single apparent diffusion coefficient is used to describe the dynamics of all films at once (dashed lines), the absorbing boundary condition model does not capture the hole transfer dynamics as accurately at these extremes as the interfacial transfer model. While the diffusion-transfer model does provide a better fit, this alone does not provide conclusive evidence for interfacial hole transfer being a major factor in this system.

To further confirm the role of interfacial hole transfer, the apparent diffusion constant was calculated for each individual $Sb_2S_3$–CuSCN film. If interfacial transfer is not a limiting factor, as assumed in this model, $D_A$ should be constant. In contrast, as shown in Fig. 8B, we observe that $D_A$ increases with increasing film thickness. This behavior can be explained because interfacial transfer plays a more dominant role in decreasing hole transfer kinetics in thin films than in thick films. Together with the improved fit obtained using the diffusion-transfer model, the increase of $D_A$ with $Sb_2S_3$ thickness clearly demonstrates the important role interfacial hole transfer plays in the $Sb_2S_3$–CuSCN system. This confirms the validity of the results obtained from the previous diffusion-transfer model.

A comparison of the diffusion-transfer and diffusion-only models provides strong evidence that interfacial transfer limits the observed hole transfer dynamics. Nevertheless, analysis using absorbing boundary conditions can provide a useful estimate of the productive absorber thickness through the calculation of the apparent diffusion length, $L_{DA}$, as shown in Fig. 8C. By neglecting interfacial hole transfer limitations in this model, $L_{DA}$ combines the contributions of diffusion, interfacial

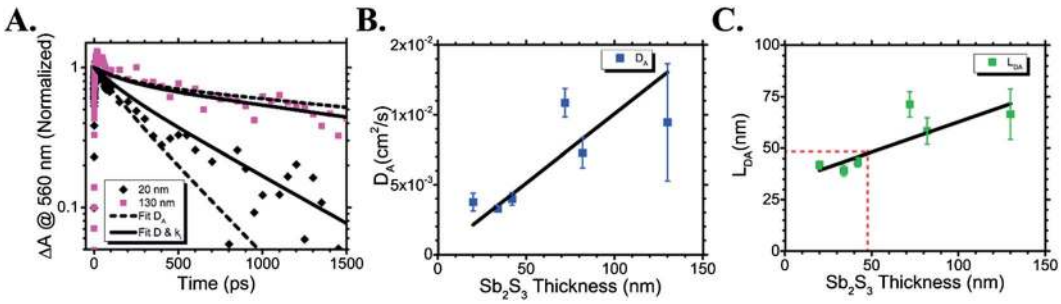


Fig. 8 (A) Plot of the modeled transient absorption response with (solid line) and without (dashed line) accounting for interfacial hole transfer for 20 nm and 130 nm $Sb_2S_3$ films. The sum of the square of residuals for all films was calculated as $\varepsilon_{Dk} = 1.66 \times 10^{-4}$ and $\varepsilon_D = 1.76 \times 10^{-4}$ with and without accounting for interfacial hole transfer, respectively. (B) Apparent diffusion coefficient, $D_A$, with changing $Sb_2S_3$ thickness neglecting interfacial hole transfer. The increase in $D_A$ is attributed to the effect of interfacial hole transfer limitations. (C) Plot of $L_{DA}$ *vs.* $Sb_2S_3$ thickness modeled linearly which shows the estimate of productive absorber thickness of ~50 nm where $L_{DA}$ is equal to $Sb_2S_3$ thickness.

 

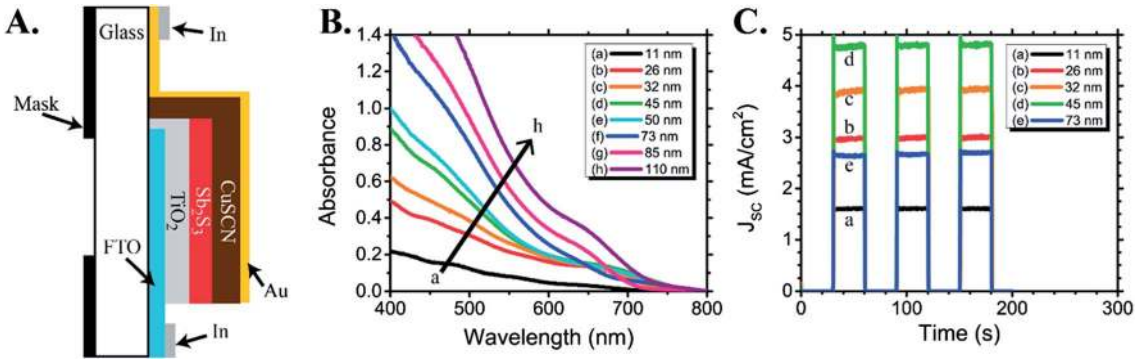


Fig. 9 (A) Scheme showing the $TiO_2$–$Sb_2S_3$–CuSCN solar cell. (B) UV-visible absorption spectra of $TiO_2$–$Sb_2S_3$ solar cells showing $Sb_2S_3$ thickness layer calculated from the film absorption at 450 nm. (C) Short-circuit photocurrent density obtained with solar cells containing $Sb_2S_3$ layers (a) 11 nm, (b) 26 nm, (c) 32 nm, (d) 45 nm, and (e) 73 nm thick. Other solar cells studied not shown for clarity.

transfer, and recombination into a single device specific parameter. Therefore, the productive absorber thickness was calculated by fitting the change of $L_{DA}$ with thickness linearly and determining the point at which $L_{DA}$ is equal to $Sb_2S_3$ thickness. Using this method, the productive absorber thickness was estimated as ~50 nm. This is not a rigorous calculation, but gives an estimate of the maximum $Sb_2S_3$ thickness that should be employed in a photovoltaic device to balance charge extraction and light absorption. This is significantly lower than the carrier diffusion length, $L_D = 180 \pm 60$ nm, because of interfacial hole transfer limitations.

### Photovoltaic performance

As seen both from transient absorption kinetics data and a modeling of the hole transfer process, thicker $Sb_2S_3$ films exhibit slower hole transfer due to charge carrier diffusion. However, it is not clear that this slower hole transfer will be detrimental to actual solar cell performance as device parameters are governed by a wide array of competing processes.[47,48] Therefore, to explore the significance of this observation with respect to $Sb_2S_3$ photovoltaics, $TiO_2$–$Sb_2S_3$–CuSCN solar cells were constructed as shown in Fig. 9A with $Sb_2S_3$ films of varying thickness on planar nonporous $TiO_2$ substrates. UV-visible absorption spectra of the solar cells are shown in Fig. 9B before CuSCN deposition. The short-circuit current density ($J_{SC}$) of these solar cells measured under 100 mW $cm^{-2}$ AM 1.5G simulated solar irradiation is presented in Figure 9C. $J_{SC}$ increases initially with increasing $Sb_2S_3$ thickness due to increased light absorption. On the other hand, as the thickness of the $Sb_2S_3$ layer increases further, the kinetics of hole transfer are decreased by hole diffusion which increases electron–hole recombination, and consequently $J_{SC}$ begins to decrease.

The photocurrent maximum was observed for the device with a 45 nm $Sb_2S_3$ film which correlates very well with the estimate of the productive absorber thickness of ~50 nm, as calculated from $L_{DA}$. This agreement further establishes the power of diffusion analysis with absorbing boundary conditions for providing an estimation of the maximum critical absorber dimension in a photovoltaic device. In comparison, $L_D$ is almost four times this value because it is an estimation of diffusion only, so it does not capture the interfacial hole transfer limitations which serve to decrease the productive absorber thickness below the diffusion limited value.

To further establish the link between photocurrent and hole transfer kinetics, we conducted external quantum efficiency (EQE) measurements shown in Fig. 10A. From these measurements, the internal quantum efficiency (IQE) was calculated based on eqn (22) to correct for solar cell absorbance.

$$\mathrm{IQE} = \mathrm{EQE}/\mathrm{LHE} \tag{22}$$

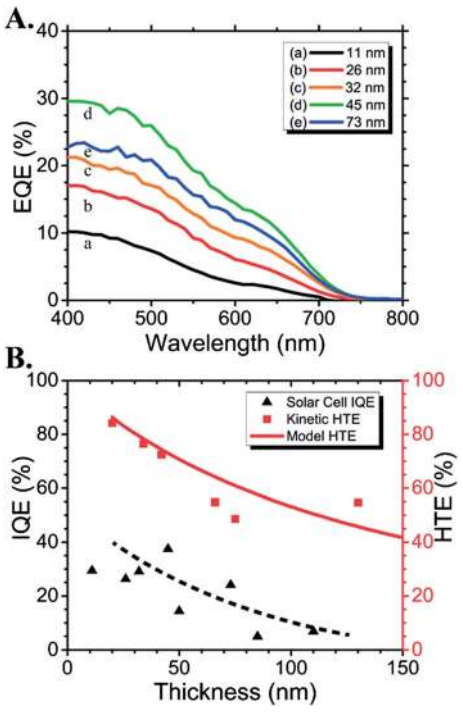


Fig. 10 (A) External quantum efficiency (EQE) measured for solar cells with $Sb_2S_3$ layers (a) 11 nm, (b) 26 nm, (c) 32 nm, (d) 45 nm, and (e) 73 nm thick. (B) Comparison of the internal quantum efficiency (IQE, triangles, left ordinate) at 450 nm and hole transfer efficiency (HTE, squares, right ordinate) as a function of $Sb_2S_3$ layer thickness.

where LHE is the light harvesting efficiency or the percent of incident light absorbed by the solar cell. IQE provides a measurement of the efficiency with which absorbed photons are converted to photocurrent. The average IQE from 450–550 nm was compared to the hole transfer efficiency (HTE), shown in Fig. 10B. HTE is calculated from the hole transfer kinetic data *via* eqn (23).

$$\mathrm{HTE} = k_{\mathrm{ht}}/(\langle\tau\rangle_{\mathrm{Sb_2S_3}}{}^{-1} + k_{\mathrm{ht}}) \quad (23)$$

where $k_{\mathrm{ht}}$ is the rate of hole transfer, and $\langle\tau\rangle_{\mathrm{Sb_2S_3}}$ is the average lifetime of the $S^{-\bullet}$ induced absorption without CuSCN.

These results show that solar cell IQE closely follows the HTE calculated by transient absorption spectroscopy. From this, we conclude that HTE is a very important contributing factor to the efficiency of charge extraction in $TiO_2$–$Sb_2S_3$–CuSCN photovoltaics. However, IQE was lower in all cases than HTE for similar $Sb_2S_3$ thickness, implying that other factors such as back electron transfer, inefficient charge collection, and inefficient electron extraction also contribute to the lower IQE.

# Conclusions

This study comprehensively investigates the role and mechanism of hole transfer in solid-state $Sb_2S_3$ solar cells. Due to diffusion of holes in the $Sb_2S_3$ films, the observed hole transfer rate, as measured by femtosecond transient absorption spectroscopy, decreased over an order of magnitude from $1.15 \pm 0.6 \times 10^9$ $s^{-1}$ for 20 nm thick $Sb_2S_3$ films to $2.6 \pm 0.8 \times 10^8$ $s^{-1}$ for 130 nm thick films. We show that the hole transfer dynamics, including the hole transfer rate, is adequately described for all of these $Sb_2S_3$–CuSCN films by an effective hole diffusion coefficient and interfacial hole transfer coefficient. From this it was shown, by calculation of the hole transfer Biot number ($\lambda$), that both diffusion and interfacial transfer are important in dictating the overall hole transfer rate in this system ($\lambda \sim 1$). However, high efficiency $Sb_2S_3$ photovoltaics utilize mesoporous $TiO_2$ substrates with high surface roughness so that the $Sb_2S_3$ layer is generally less than 20 nm.[17] For a 20 nm $Sb_2S_3$ film the hole transfer Biot number is estimated as $\lambda = 0.10 \pm 0.01$. This low Biot number implies that interfacial transfer is the rate limiting step for hole transfer in these devices.

Confirmation of the role of interfacial transfer is seen by employing a simplified model that neglects interfacial hole transfer limitations through absorbing boundary conditions. This simplified model is unable to adequately fit the time-resolved kinetic data for $Sb_2S_3$ and predicts an increasing diffusion constant with increasing $Sb_2S_3$ thickness. In spite of this, it is shown that this simplified model provides an accurate prediction of productive absorber thickness, 50 nm, from the apparent diffusion length, $L_{\mathrm{DA}}$, by combining diffusion, interfacial transfer, and recombination effects into one parameter. This result was confirmed through the construction of planar photovoltaics in which the peak short-circuit current was observed with a 45 nm $Sb_2S_3$ layer. In addition, planar $Sb_2S_3$ photovoltaics demonstrate that hole transfer is an important limiting parameter in photovoltaic performance.

In summary, it is shown that interfacial hole transfer, not mobility, is the most important parameter limiting the productive absorber thickness and hole transfer rate in high efficiency $Sb_2S_3$ photovoltaics. In addition, we provide an estimate of hole mobility ($\mu = 2.6 \pm 1.9$ $cm^2$ $V^{-1}$ $s^{-1}$) in $Sb_2S_3$ under experimental conditions closely resembling those of an actual solar cell. Understanding the mechanism by which hole transfer is controlled is important for the further optimization of materials and interfaces in these photovoltaics. Therefore, it is crucial to take into account transfer across the donor/acceptor interface to obtain an accurate picture of the processes involved.

# Experimental methods

### Materials

Antimony chloride ($SbCl_3$, Alfa Aesar, 99%), copper(I) thiocyanate (CuSCN, Strem Chemicals, 99%), di-*n*-propyl sulfide ($C_6H_{14}S$, Alfa Aesar, 98%), potassium thiocyanate (KSCN, Aldrich, 99%), sodium thiosulfate pentahydrate ($Na_2S_2O_3 \cdot 5H_2O$, Alfa Aesar, 99%), titanium diisopropoxide bis(acetylacetonate) ($[(CH_3)_2CHO]_2Ti(C_6H_7O_2)_2$, Sigma Aldrich, 75 wt% in isopropanol), and zinc powder (median 6–9 μm, Alfa Aesar, 97.5%) were used without further purification.

### Preparation of $Sb_2S_3$ films for transient absorption spectroscopy

Glass microscope slides (2 cm × 0.7 cm) were cleaned in a detergent solution in an ultrasonic bath for 15 min, rinsed with water and ethanol, and heated at 500 °C for 5 min. A compact $TiO_2$ layer (~150 nm) was deposited by spray pyrolysis from a 0.2 M solution of titanium diisopropoxide bis(acetylacetonate) in ethanol at 400 °C.[49] Deposition of $Sb_2S_3$ was carried out by chemical bath deposition (CBD) at 7 °C for 20–90 min.[24] The slides were removed, rinsed with water, and then dried with a soft stream of air. The as-deposited films were annealed under nitrogen for 20 min at 300 °C until they turned to dark brown, crystalline, stibnite. After annealing, films were stored in dry air until further characterization. Following characterization of the $TiO_2$–$Sb_2S_3$ films, a CuSCN layer was applied to be able to compare identical $Sb_2S_3$ films with and without CuSCN. Before CuSCN application, the $Sb_2S_3$ films were immersed in a 0.5 M aqueous KSCN solution for 5 min. The films were removed and excess KSCN was wicked away. 10 μL $cm^{-2}$ of 0.05 M CuSCN solution in di-*n*-propyl sulfide was deposited at 15 μL $min^{-1}$ while the deposition needle was moved over the film at 1 mm $s^{-1}$. The substrate was placed on a hotplate at 80 °C and deposition was carried out using a homemade deposition apparatus similar to that reported by O'Regan *et al.*[50] The completed films were then stored in dry air until further characterization.

### Fabrication of solar cells

A portion of the fluorine doped tin oxide (FTO) glass substrates (Pilkington Glass, TEC-7, 2 mm thickness) were masked and a thin layer of Zn powder was applied on the unmasked section. Concentrated HCl was dripped over the Zn powder and allowed

 

to sit for approximately 10 s to completely etch away the FTO layer before washing with $H_2O$. The etched FTO substrates (2 cm $\times$ 1.5 cm) were then cleaned and $TiO_2$, $Sb_2S_3$, were deposited as described above for the $Sb_2S_3$ films used for transient absorption spectroscopy. 40 μL $cm^{-2}$ of 0.05 M CuSCN solution was deposited at 20 μL $min^{-1}$ in the same way as for transient absorption films. To complete the solar cell, an Au contact (100 nm) was evaporated on the CuSCN to form the back electrical contact. The solar cell active area was masked (typically ~0.10 $cm^2$) and the precise active area was determined using ImageJ image analysis software.[51] Complete solar cells were illuminated at open-circuit under 100 mW $cm^{-2}$ AM 1.5G irradiation for 2 h before measurement.[16]

**Optical, and photovoltaic characterization.** UV-visible absorption spectra were recorded using a Varian Cary 50 Bio spectrophotometer. A 300 W Xe lamp with an AM 1.5G filter was used to irradiate the solar cells at 100 mW $cm^{-2}$ and short-circuit current measurements were carried out using a Princeton Applied Research 2273 (PARstat) potentiostat. Incident photo to carrier efficiencies (IPCE) were measured using a Newport Oriel QE/IPCE measurement kit with a silicon photodiode reference detector.

**Femtosecond transient absorption.** Femtosecond transient absorption measurements of $TiO_2$–$Sb_2S_3$ and $TiO_2$–$Sb_2S_3$–CuSCN films were conducted using a Clark MXR 2010 (775 nm, 1 mJ per pulse, fwhm pulse width = 130 fs, 1 kHz repetition rate) and an Ultrafast Systems (Helios) UV-visible detection system. The fundamental laser output was split into pump (95%) and probe (5%) beams. The pump beam was directed through a second harmonic frequency doubler to produce the 387 nm pump beam and the probe beam passed through an optical delay rail and was focused on a Ti:sapphire crystal to produce a white light continuum. The pump was attenuated at 40 μJ per pulse and the optical delay stage provided a probe time window of 1.6 ns with a step resolution of 7 fs. Kinetic traces were assembled at the appropriate wavelengths from the time-resolved spectral data. All films studied were placed in evacuated quartz cells for measurement.

## Acknowledgements

The research described herein was supported by the Division of Chemical Sciences, Geosciences, and Biosciences, Office of Basic Energy Sciences of the U.S. Department of Energy through award DE-FC02-04ER15533. This is contribution number NDRL no. 4993 from the Notre Dame Radiation Laboratory.

## References

1 P. V. Kamat, *J. Phys. Chem. Lett.*, 2013, **4**, 908–918.
2 P. V. Kamat, *J. Phys. Chem. C*, 2007, **111**, 2834–2860.
3 N. Park, *J. Phys. Chem. Lett.*, 2013, **4**, 2423–2429.
4 M. Grätzel, *Nature*, 2001, **414**, 338–344.
5 G. Hodes and D. Cahen, *Acc. Chem. Res.*, 2012, **45**, 705–713.
6 B. Li, L. Wang, B. Kang, P. Wang and Y. Qiu, *Sol. Energy Mater. Sol. Cells*, 2006, **90**, 549–573.
7 M. Grätzel, *C. R. Chim.*, 2006, **9**, 578–583.
8 P. P. Boix, G. Larramona, A. Jacob, B. Delatouche, I. Mora-Seró and J. Bisquert, *J. Phys. Chem. C*, 2012, **116**, 1579–1587.
9 C. Lévy-Clément, R. Tena-Zaera, M. A. Ryan, A. Katty and G. Hodes, *Adv. Mater.*, 2005, **17**, 1512–1515.
10 I. Mora-Seró, S. Giménez, F. Fabregat-Santiago, E. Azaceta, R. Tena-Zaera and J. Bisquert, *Phys. Chem. Chem. Phys.*, 2011, **13**, 7162–7169.
11 Y. Zou, D. Li, X. Sheng, L. Wang and D. Yang, *Sol. Energy*, 2012, **86**, 1359–1365.
12 G. Larramona, C. Choné, A. Jacob, D. Sakakura, B. Delatouche, D. Péré, X. Cieren, M. Nagino and R. Bayón, *Chem. Mater.*, 2006, **18**, 1688–1696.
13 A. Belaidi, T. Dittrich, D. Kieven, J. Tornow, K. Schwarzburg and M. Lux-Steiner, *Phys. Status Solidi RRL*, 2008, **2**, 172–174.
14 J. A. Chang, S. H. Im, Y. H. Lee, H.-J. Kim, C.-S. Lim, J. H. Heo and S. Il Seok, *Nano Lett.*, 2012, **12**, 1863–1867.
15 P. P. Boix, Y. H. Lee, F. Fabregat-Santiago, S. H. Im, I. Mora-Sero, J. Bisquert and S. Il Seok, *ACS Nano*, 2012, **6**, 873–880.
16 S. Nezu, G. Larramona, C. Choné, A. Jacob, B. Delatouche, D. Péré and C. Moisan, *J. Phys. Chem. C*, 2010, **114**, 6854–6859.
17 Y. Itzhaik, O. Niitsoo, M. Page and G. Hodes, *J. Phys. Chem. C*, 2009, **113**, 4254–4256.
18 S.-J. Moon, Y. Itzhaik, J.-H. Yum, S. M. Zakeeruddin, G. Hodes and M. Grätzel, *J. Phys. Chem. Lett.*, 2010, **1**, 1524–1527.
19 K. Tsujimoto, D. Nguyen, S. Ito, H. Nishino, H. Matsuyoshi, A. Konno, G. R. A. Kumara and K. Tennakone, *J. Phys. Chem. C*, 2012, **116**, 13465–13471.
20 J. A. Chang, J. H. Rhee, S. H. Im, Y. H. Lee, H. Kim, S. Il Seok, M. K. Nazeeruddin and M. Gratzel, *Nano Lett.*, 2010, **10**, 2609–2612.
21 T. Fujita, K. Kurita, K. Takiyama and T. Oda, *J. Phys. Soc. Jpn.*, 1987, **56**, 3734–3739.
22 F. T. F. O'Mahony, T. Lutz, N. Guijarro, R. Gómez and S. A. Haque, *Energy Environ. Sci.*, 2012, **5**, 9760–9764.
23 N. Bansal, F. T. F. O'Mahony, T. Lutz and S. A. Haque, *Adv. Energy Mater.*, 2013, **3**, 986–990.
24 J. A. Christians and P. V. Kamat, *ACS Nano*, 2013, **7**, 7967–7974.
25 B. Kippelen and J.-L. Brédas, *Energy Environ. Sci.*, 2009, **2**, 251–261.
26 G. Xing, N. Mathews, S. Sun, S. S. Lim, Y. M. Lam, M. Gratzel, S. Mhaisalkar and T. C. Sum, *Science*, 2013, **342**, 344–347.
27 S. D. Stranks, G. E. Eperon, G. Grancini, C. Menelaou, M. J. P. Alcocer, T. Leijtens, L. M. Herz, A. Petrozza and H. J. Snaith, *Science*, 2013, **342**, 341–344.
28 A. M. Goodman, *J. Appl. Phys.*, 1961, **32**, 2550–2552.
29 T. Stübinger and W. Brütting, *J. Appl. Phys.*, 2001, **90**, 3632–3641.
30 H. Najafov, B. Lee, Q. Zhou, L. C. Feldman and V. Podzorov, *Nat. Mater.*, 2010, **9**, 938–943.
31 D. Zhitomirsky, O. Voznyy, S. Hoogland and E. H. Sargent, *ACS Nano*, 2013, **7**, 5282–5290.
32 A. Huijser, T. J. Savenije, S. C. J. Meskers, M. J. W. Vermeulen and L. D. A. Siebbeles, *J. Am. Chem. Soc.*, 2008, **130**, 12496–12500.

33 S. N. Clafton, D. M. Huang, W. R. Massey and T. W. Kee, *J. Phys. Chem. B*, 2013, **117**, 4626–4633.
34 P. E. Shaw, A. Ruseckas and I. D. W. Samuel, *Adv. Mater.*, 2008, **20**, 3516–3520.
35 J. Burschka, N. Pellet, S.-J. Moon, R. Humphry-Baker, P. Gao, M. K. Nazeeruddin and M. Grätzel, *Nature*, 2013, **499**, 316–319.
36 M. Liu, M. B. Johnston and H. J. Snaith, *Nature*, 2013, **501**, 395–398.
37 J. Z. Zhang, *J. Phys. Chem. B*, 2000, **104**, 7239–7253.
38 C. Ghosh and B. P. Varma, *Thin Solid Films*, 1979, **60**, 61–65.
39 A. M. Karguppikar and A. G. Vedeshwar, *Phys. Lett. A*, 1987, **126**, 123–126.
40 D. R. James, Y.-S. Liu, P. De Mayo and W. R. Ware, *Chem. Phys. Lett.*, 1985, **120**, 460–465.
41 J. Kirkpatrick, P. E. Keivanidis, A. Bruno, F. Ma, S. A. Haque, A. Yarstev, V. Sundstrom and J. Nelson, *J. Phys. Chem. B*, 2011, **115**, 15174–15180.
42 A. Faghri, Y. Zhang and J. R. Howell, *Advanced Heat and Mass Transfer*, Global Digital Press, Columbia, MO, 2010.
43 O. Savadogo and K. C. Mandal, *J. Electrochem. Soc.*, 1994, **141**, 2871–2877.
44 D. E. Mears, *Ind. Eng. Chem. Process Des. Dev.*, 1971, **10**, 541–547.
45 Y. Xu and Y. Zhang, *Atmos. Environ.*, 2003, **37**, 2497–2505.
46 D. Bi, L. Yang, G. Boschloo, A. Hagfeldt and E. M. J. Johansson, *J. Phys. Chem. Lett.*, 2013, **4**, 1532–1536.
47 K. Tvrdy, P. A. Frantsuzov and P. V. Kamat, *Proc. Natl. Acad. Sci. U. S. A.*, 2011, **108**, 29–34.
48 V. Chakrapani, D. R. Baker and P. V. Kamat, *J. Am. Chem. Soc.*, 2011, **133**, 9607–9615.
49 L. Kavan and M. Grätzel, *Electrochim. Acta*, 1995, **40**, 643–652.
50 B. C. O'Regan and F. Lenzmann, *J. Phys. Chem. B*, 2004, **108**, 4342–4350.
51 C. A. Schneider, W. S. Rasband and K. W. Eliceiri, *Nat. Methods*, 2012, **9**, 671–675.

 